Z. Phys. A 359, 277–290 (1997)

ZEITSCHRIFT
FÜR PHYSIK A

Multifragmentation of Gold nuclei in the interactions with photoemulsion nuclei at 10.7 GeV/nucleon

EMU-01/12 – collaboration

M.I.Adamovich[14], **M.M.Aggarwal**[4], **Y.A.Alexandrov**[14], **R.Amirikas**[18], **N.P.Andreeva**[1], **Z.V.Anzon**[1], **F.A.Avetyan**[22], **S.K.Badyal**[9], **A.M.Bakich**[18], **E.Baklitskaya**[20], **E.S.Basova**[19], **K.B.Bhalla**[8], **A.Bhasin**[9], **V.S.Bhatia**[4], **V.G.Bogdanov**[17], **V.Bradnova**[7], **V.I.Bubnov**[1], **X.Cai**[21], **I.Y.Chasnikov**[1], **G.M.Chen**[2], **L.P.Chernova**[20], **M.M.Chernyavsky**[14], **S.Dhamija**[4], **K.El Chenawi**[12], **G.Z.Eligbaeva**[1], **L.E.Eremenko**[1], **D.Felea**[3], **S.Q.Feng**[21], **A.S.Gaitinov**[1], **E.R.Ganssauge**[13], **S.Garpman**[12], **S.G.Gerassimov**[14], **A.Gheata**[3], **M.Gheata**[3], **J.Grote**[15], **K.G.Gulamov**[20], **S.K.Gupta**[8], **V.K.Gupta**[9], **M.Haiduc**[3], **D.Hasegan**[3], **U.Henjes**[13], **B.Jakobsson**[12], **L.Just**[10], **G.S.Kalyachkina**[1], **E.K.Kanygina**[1], **M.Karabova**[10], **S.P.Kharlamov**[14], **A.D.Kovalenko**[7], **S.A.Krasnov**[7], **V.Kumar**[8], **V.G.Larionova**[14], **Y.X.Li**[5], **L.S.Liu**[21], **Z.G.Liu**[5], **S.Lokanathan**[8], **J.J.Lord**[15], **N.S.Lukicheva**[20], **Y.Lu**[2], **S.B.Luo**[11], **L.K.Mangotra**[9], **I.Manhas**[9], **N.A.Marutyan**[22], **A.Y.Mashkov**[20], **N.V.Maslennikova**[14], **I.S.Mittra**[4], **A.K.Musaeva**[1], **S.Z.Nasyrov**[19], **V.S.Navotny**[20], **J.Nystrand**[12], **G.I.Orlova**[14], **I.Otterlund**[12], **L.S.Peak**[18], **N.G.Peresadko**[14], **N.V.Petrov**[19], **V.A.Plyushchev**[17], **W.Y.Qian**[21], **Y.M.Qin**[11], **R.Raniwala**[8], **N.K.Rao**[9], **J-T. Rhee**[16], **M.Roeper**[13], **V.V.Rusakova**[7], **N.Saidkhanov**[20], **N.A.Salmanova**[14], **L.G.Sarkisova**[22], **V.R.Sarkisyan**[22], **A.M.Seitimbetov**[1], **R.Sethi**[4], **C.I.Shakhova**[1], **B.Singh**[8], **D.Skelding**[15], **K.Soderstrom**[12], **E.Stenlund**[12], **L.N.Svechnikova**[20], **T.Svensson**[12], **A.M.Tawfik**[13], **M.Tothova**[10], **M.I.Tretyakova**[14], **T.P.Trofimova**[19], **U.I.Tuleeva**[19], **B.P.Tursunov**[19], **V.V.Uzhinskii**[6], **Vani Vashisht**[4], **S.Vokal**[10], **J.Vrlakova**[10], **H.Q.Wang**[12,21], **S.H.Wang**[2], **X.R.Wang**[21], **Z.Q.Weng**[5], **R.J.Wilkes**[15], **C.B.Yang**[21], **Z.B.Yin**[21], **L.Z.Yu**[21], **D.H.Zhang**[11], **P.Y.Zheng**[2], **S.I.Zhokhova**[20], **D.C.Zhou**[21]

[1] High Energy Physics Institute, Almaty, Kazakhstan
[2] Institute of High Energy Physics, Academia Sinica, Beijing, China
[3] Institute of Gravitation and Space Research, Bucharest,Romania
[4] Department of Physics,Panjab University, Chandigarh, India
[5] Department of Physics, Hunan Education Institute, Changsha, Hunan,China
[6] Lab. of Comp. Technics, Joint Institute for Nuclear Research (JINR), Dubna, Russia
[7] Lab. of High Energies, Joint Institute for Nuclear Research (JINR), Dubna, Russia
[8] Department of Rhysics, University of Rajasthan, Jaipur, India
[9] Department of Physics, University of Jammu, Jammu, India
[10] Department of Nuclear Physics and Biophysics, Safarik University,Kosice, Slovakia
[11] Department of Physics, Shanxi Normal University, Linfen, Shanxi, China
[12] Department of Physics, University of Lund, Lund, Sweden
[13] F.B.Physik, Philipps University, Marburg, Germany
[14] P.N. Lebedev Physical Institute, Moscow, Russia
[15] Department of Physics, University of Washington, Seattle, Washington, USA
[16] Department of Physics, Konkuk University, Seoul, Korea
[17] V.G.Khlopin Radium Institute, St. Petersburg, Russia
[18] School of Physics, University of Sydney, Sydney, Australia
[19] Lab. of Rel. Nuclear Physics, Institute of Nuclear Physics, Tashkent, Uzbekistan
[20] Lab. of High Energies, Physical-Technical Institute, Tashkent, Uzbekistan
[21] Institute of Particle Physics, Hua-Zhong Normal University, Wuhan, Hubei, China
[22] Yerevan Physics Institute, Yerevan, Armenia

Received: 22 July 1997
Communicated by V.V. Anisovich

Abstract. Recent results from the EMU-01/12 collaboration are presented for 10.7 GeV/nucleon gold nuclei interactions in emulsion. The distributions of "bound" charge (Z_{bound}, Z_{b3}), multiplicity distributions, fragment correlations and fluctuations are discussed. The data are compared to similar results obtained on the ALADIN setup at 600 MeV/nucleon. It is shown that multifragmentation of gold nuclei at high and intermediate energies has common features. It is also obtained that the IMFs have reduced multiplicity at high energies.

The data are analyzed within the scope of the statistical model of multifragmentation. This model requires the following predetermined model ingredients: mass, charge and excitation energy of nuclear residuals. The simple estimation method of these characteristics is proposed in the framework of the Glauber approach. It is shown that the multifragmentation model reproduces qualitatively the present data. A dramatic discrepancy between the predicted and experimental yield of two charged fragments is found. The evolution of transverse momentum of fragments as a function of Z_{bound} is presented. It is shown that the model greatly underpredicts the transverse momentum of fragments. It is interpreted as evidence of a strong radial flow of spectator fragments.

PACS: 25.70.Pq; 25.75.+r; 24.85.+p

1 Introduction

The dominating decay mode of weakly excited heavy nuclei is emission (evaporation) of neutrons and light nuclei (protons, deutrons, tritium and helium). Highly excited nuclei, as a rule, are broken to yield a few intermediate mass fragments (IMF) ($3 \leq Z_F \leq 30$). Such fragments can hardly be expected to be products either evaporation or a series of subsequent asymmetric breakup. Because of this, there arose a picture of "explosive", simultaneous nuclear breakup into several fragments and, as a consequence, the need for understanding the mechanism of the process like that.

The most common standpoint is that multifragmentation is a statistical process. So, the popular models [1,2] suggest that breakup of highly excited nuclei is governed by general statistical regularities. In particular, the probability of a given N fragment mode occurring is proportional to $\int \exp(S) d^{3N}p d^{3N}r$, where S - the entropy of the system, and the integration is carried out over an accessible phase volume of N particles. S interpreted as the entropy of non-interecting "hot" [1] or "cold" [2] nuclei. To determine the accessible phase volume, it is necessary to introduce the energy of the fragmenting system and its volume. The system energy can generally be estimated experimentally. As for the volume, it is an fitting parameter and its value may be taken as the volume occupied by the system at the instant interfragment interactions may be ignored. Entering the volume in excess of that of the "ground" state by factor 3 allowed the authors of [3] to describe successfully the findings of the ALADIN-experiment [3-6][1] in terms of the statistical model [1], which is undisputably a serious argument in support of the statistical approach.

More conservative advances have been made in the scope of the models of molecular dynamics [7] and quantum molecular dynamics (QMD) [8] following the progression of nuclear reactions from the first to the final stage. The models involve predetermined forces acting between nucleons and calculated trajectories of all particles. In addition, it is necessary to preset a criterion of nucleon joining into "cluster-fragment". This problem is known even in the classical statistical physics (see [9]). One of the solutions of the theory of nuclear reactions produces the result - prototypes, "germs" of fragments originate at the early stage of the reaction [10]. In the course of the interaction the nucleonic composition and kinematic characteristics of a fragment undergo a change both because of the interaction with other fragments and because of gaining or losing some nucleons and clusters[2]. In other words, by the model, multifragmentation is an intricate evolutional process.

Experimental evidence as it stands at present gives no way of preferring a certain point of view. In such a situation, we believe that the experimental investigation of the thermalization degree of the fragment system is advantageous.

The simplest criterion of the system thermalization must be the independence of fragment energies of their sizes. Under thermal equilibrium the average kinetic energies of different kinds of particles in the mixture of ideal gases must be equal. Rough permanence of fragment energies was shown [12] for proton interactions with Au-nuclei. In the central collisions of heavy nuclei, the so-called radial flow of fragments [13] - the proportionality of a fragment energy to its size - is observed. The availability of the flow is interpreted as evidence for forming severely compressible nuclear substance in collisions. It can seemingly represented by transport models. However, within the framework of the statistical approach collective motions in the fragmenting system can also be taken into account. Examined in [14] was the influence of the angular momentum of nuclear residuals on the multifragmentation characteristics. It has been shown that an increase in the angular momentum of nuclear residuals gives rise to decreasing the IMFs multiplicity and increasing fragment energies. It is but natural that the angular momentum of nuclear residuals leads to decay anysotropy and, thus, of interest is the study of the angular isotropy of fragments.

Compared to at intermediate energies, decreased multiplicity of fragments at high energies has been found in collisions of Au-nuclei with emulsion at energy above 1 A GeV [15,16]. The authors of this work, however, failed to analyze the energetic and angular spectra of fragments, which can provide information on collective flows. As of today, an intense experimental and theoretical work is dedicated to studying anysotropy of light nuclei emission (see, for example, [17]) and much less is known about the anysotropy of nuclear multifragmentation and multifragmentation dependence on collision centrality. This investigation is the aim of the present work. To do this, we used our measurements of 10.7 A GeV Au-nuclei interactions in emulsion. The information about experimental material and experimental procedures are summarized in Sect. 2.

Similar data have been presented elsewhere [15,16]. The authors used the value Z_{bound} - the sum of all charges with $Z_F \geq 2$ - to estimate the charge of fragmenting nucleus. Such a recipe has been given in the papers of the ALADIN-collaboration, where a considerable body of 600 A MeV gold nuclei multifragmentation information in line with predictions of a number of models has been provided. The registration conditions of the fragments with $Z \leq 4$ on the ALADIN setup and in emulsion experiments differs greatly. This fact has been ignored by authors of experiments [15,16] with the result that the reason for experimental data at high and intermediate energies being distinguishable is unclear. We would like to remember that such a disagreement may be due to either dissimilar efficiency in light fragment registration or changed mechanism of multifragmentation in passing from intermediate to high energies. This question will be discussed in Sect. 4.

In one of the works of the ALADIN-collaboration [3] the variable Z_{b3} - the sum of all fragments with $Z_F \geq 3$ was in use. Two quantities (Z_{bound} and Z_{b3}) differ by the sum of fragments with Z_F = 2. The production mechanism of fragments with $Z_F \leq 2$ is not yet completely understood [18]. This circumstance hampers the elucidation of the nuclear multifragmentation mechanism. We experimentally verified that the use of Z_{b3} instead of Z_{bound} makes possible the discrimination between the mechanisms at high and intermediate energies (see Sect. 4).

Effort to understand the origin of differing the interaction mechanism and to assess the thermalization degree of fragment system is dedicated Sect. 5, where we analyze the sphericity of events, azimuthal correlations of fragments and

[1] Also, see the description of a great body of experimental data in [1]

[2] Similar results are derived from the solution of Boltzmann-Welling-Ulenbek equation with due regard for fluctuations in the spinoidal range

the dependence of the transverse fragment momentum on Z_{bound}.

Another goal of the work - the development of methods for theoretical description of nuclear multifragmentation at high energies. A theoretical description generally starts from the assumption of two stages, phases of the interaction. It is conjectured that at first, non-equilibrium stage the occurrence of "hot", excited nuclear residuals takes place. At the second, there arises the decay of the residuals. Non-equilibrium stage lasts during the characteristic collision time of order 10^{-22}sec. It takes longer for nuclear residuals to be evaporated or broken up: $\sim 10^{-21} - 10^{-15}$ sec.

Microscopic approach - the models of molecular dynamics [8,7] or models of intranuclear cascade [19] - would use to examine the first stage of the process. To understand the second stage, statistical models are invoked. The formation of prefragments is, at times, dealt with in terms of transport models. Unfortunately, most of them is inapplicable at energies above 10.7 A GeV. The cascade model, as shown in [20], considerably overestimates the breakup of gold nuclei interacting with emulsion nuclei at 10.7 A GeV. In combination with the statistical nuclear multifragmentation model [1], the model of relativistic quantum molecular dynamics (RQMD) [21] popular at high energies have found no applications till now [22]. In view of the complexity of RQMD, we invoked a simpler Regge model of nuclear breakup [23], whose basics are briefly discussed in Sect. 3. The model enables the estimation of nuclear residual sizes and charges.

Using the relation between the residual size and its excitation energy proposed in [3], we have a good chance of completely describing the ensemble of nuclear residuals. To simulate the fragmentation of excited nuclear residuals we followed the statistical nuclear multifragmentation model [1], whose basics are also given in Sect. 3.

"Capability" of the combined model we tested by the results of the ALADIN- collaboration. After that, we could be assured that the model offers the proper extrapolation to high energies, where the model predictions had proved to be somewhat inconsistent with experimental findings.

The comparison with model predictions and the main bulk of experimental data are accumulated in Sect. 4 and 5. In particular, Sect. 4 deals with the frequency characteristics of interactions: the "bound" charge distribution, the dependence of intermediate mass fragment multiplicity on the "bound" charge, correlations between fragment multiplicities and so on. Section 5 analyzes the sphericity of events and azimuthal correlations. In particular, in Sect. 5.3 we show the dependences of kinetic fragment energies on the value of "bound" charge.

Finally, our consideration ends in brief summary in Sect. 6.

2 Experimental material

Ten stacks of NIKFI BR-2 emulsion pellicles of dimension $10 \times 10 \times 0.06cm^2$ (each containing 30 plates) were exposed to a 10 A GeV Au beam at the BNL/AGS. The sensitivity of emulsion was not worse than 30 grains per $100\mu k$ for singly charged particles with minimal ionization.

All interactions were found by along-the track "fast-slow" scanning with a velocity excluding any discrimination in the event selection. "Slow" scanning (in backward direction) was made to find events with unbiased projectile track. After excluding the events of electro-magnetic dissociation and purely elastic scattering a total of 1057 inelastic interactions were left for the investigation.

Experimentally, the spectator fragments with Z = 2 were classified by the visual inspection of tracks. The ionization of such tracks is constant over the whole length and equals g/g_0 = 4, where g_0 is the minimal ionization of singly charged track. Charge assignment for multiply charged tracks were provided by delta-electron density measurements (on the length not less 10 mm); all the fragment tracks were calibrated with known primary and two- charged tracks. From our results, the accuracy of measured charges for the fragments with $Z_F < 10$, $10 \leq Z_F < 28$, $28 \leq Z_F < 40$ and $Z_F \geq 40$ was ± 0.5, ± 1, ± 2, ± 3, respectively.

The relativistic particles emitted at $\theta < 17.2$ mrad were taken as singly charged fragments.

In each event, the polar θ and azimuthal angles φ of all charged particles were measured.

Transverse momenta of spectator fragments are defined as

$$\mid \mathbf{P} \mid = 2Z_F P_0 \sin\theta. \quad (1)$$

Here Z_F - a charge of the fragment, P_0=11.6 GeV/c - the momentum per a nucleon of the incident nucleus, and θ - the angle of fragment with respect to the incident primary track direction. The ration A_F/Z_F for fragments was assumed to be equal two.

In order to determined the measured accuracy of transverse momenta, "zero"-angles were measured (see [24]). On 100 tracks of primary nuclei (any point on the primary track may be chosen as the interaction vertex) the measurements of the presumed "one track" interaction were conducted, whose vertices were taken at random. In each conjectured event, the polar θ, plane α and dip γ angles were recorded. It has been found that the α- and γ-distributions follow the Normal distribution with dispersion

$$\sigma(\alpha) = 3.4 \cdot 10^{-4} \pm 3.0 \cdot 10^{-5} \quad rad,$$

$$\sigma(\gamma) = 6.0 \cdot 10^{-4} \pm 6.0 \cdot 10^{-5} \quad rad.$$

The average $< \theta >$ value corresponding to these dispersions must lie in the $4.3 \cdot 10^{-4} \div 7.5 \cdot 10^{-4}$ rad interval. The measured value of $< \theta_{meas} >$ =$6.1 \cdot 10^{-4} \pm 5.0 \cdot 10^{-5}$ rad fell into the required range, which speaks for suitability of the procedure employed.

The value of $< \theta_{meas} >$ shows the accuracy of polar measurements. As the average polar angle of the fragments proved to be $9.1 \cdot 10^{-3} \pm 1.1 \cdot 10^{-4}$ rad, the average relative accuracy in fragment transverse momenta measurements does not exceed 7%.

3 Models used in the study

3.1 Statistical model of multifragmentation

The statistical model of nuclear multifragmentation used in this paper was discussed at length in [1]. So we will restrict ourselves to some central concepts of the model.

The model suggests that nuclear reactions proceed in three principal stages: 1) rapid production of highly excited nuclear residuals in the time of the order of $2R_T/\upsilon_p$, where R_T - the radius of the target nucleus, and υ_p - the velocity of the incident nucleus in the target rest frame; 2) expansion and thermalization of the system of nuclear residuals accompanied by their breakup; 3) Coulomb-repulsion and de-excitation of fragments. The occurrence of the stages and criteria for their separation are omitted in the discussion.

The first stage of reactions are not treated. It is assumed that its description may be given in terms of transport models (QMD - models, cascade model and so on). These models are expected to predict the realistic nuclear residuals distribution (intermediate nuclear systems) of mass(A_0), charge (Z_0) and excitation energy (ϵ^*) distributions. The required distribution may also be given phenomenologically (see [3]).

The dynamics of nuclear residual expansion, e.g. an incident nucleus, is left out but it is suggested that during this stage the formation of fragments accompanied by intense exchange of nucleons, energy and momenta between the fragments is under way. Most likely, such exchanges has a stochastic character, resulting in thermalization of the system. Clearly, with increasing the mean spacing between fragments, the exchange intensity will fall and, from some time on, one can say about the system of the near-free fragments. Thereafter the fragment characteristics are practically unaffected - "freeze-out". Correspondingly, this point in time is called "freeze-out" time, and the volume of the system-breakup volume (V_b).

As can be readily appreciated, it is difficult if not impossible to refine the details of the described picture experimentally and to test its validity. Fortunately, the model uses little or no it.

The central and key tenet of the model is the assumption that the system of "hot" fragments can be represented in terms of the classical statistical mechanics involving the concepts: volume, density, temperature, particle energy, interaction potential, two-and multiparticle correlators.

The above pattern of the evolution are invoked to extend the concept of volume. Obviously, the volume is a free parameter of the model. The volume is generally [1] defined as $V_b = (1+k)V_0$, $k \sim$ 2–3, and V_0 - the volume of A_0 nucleon system in the "ground" state. We used the value of k = 2. Accordingly, the system density is – A_0/V_b.

The temperature is assumed in the usual classical sense.

The energies of particles are determined by specific nuclear information. The free energy of a fragment with mass A and charge Z at $A > 4$ is expressed by [1]

$$F_{AZ} = F^V_{AZ} + F^S_{AZ} + F^{Sym}_{AZ} + F^C_{AZ} + F^t_{AZ}, \quad (2)$$

$$F^V_{AZ} = (-W - T^2/\varepsilon_0)A, \quad (3)$$

$$F^S_{AZ} = 4\pi R^2_{AZ}\sigma(T) \equiv \beta(T)A^{2/3}, \quad (4)$$

$$\beta(T) = \beta_0 \left(\frac{T_c^2 - T^2}{T_c^2 + T^2}\right)^{5/4}, \quad (5)$$

$$F^{Sym}_{AZ} = \gamma\frac{(A-2Z)^2}{A}, \quad (6)$$

$$F^C_{AZ} = \frac{3}{5}\frac{Z^2e^2}{R_{AZ}}\left[1 - (1+\kappa_c)^{-1/3}\right]. \quad (7)$$

F^V_{AZ} - the free volume energy calculated in the Fermi gas model at low temperatures. F^S_{AZ} - the free surface energy, $\sigma(T)$ - the coefficient of the surface tension. $R_{AZ} = 1.17A^{1/3}$ - the radius of a fragment (it is assumed that fragments are spherical). T_c = 18 (MeV) - the critical temperature. F^{Sym}_{AZ} - the symmetry energy analogous to the corresponding term in the Bethe-Weizsaecker formula. The Coulomb interaction of all fragment system is considered by Wigner-Seitz approximation (see [1]). F^t_{AZ} - the translation energy calculated in the usual fashion. For light fragments ($n, p, {}^2H, {}^3H, {}^3He, {}^4He$), it is taken only translation and Coulomb energies into account. The values of parameters are given in [1].

The free energy of the fragment system is defined as

$$F_f = \sum (A,Z)F_{AZ} + \frac{3}{5}\frac{Z_0^2e^2}{r_0A_0^{1/3}(1+\kappa_c)^{1/3}}.$$

With its knowledge, it is possible to arrive at the energy and entropy of the system

$$E = F_f - T\frac{\partial F_f}{\partial T}, \quad (8)$$

$$S_f = -\frac{\partial F_f}{\partial T}. \quad (9)$$

Given the energy of the system and separation of A_0 nucleons into fragments, the (8) makes possible to find the temperature. The (9) allows the system entropy and decay channel probability to be determined

$$W_f \sim exp(S_f).$$

After examining a variety of A_0 nucleon system broken up into fragments and determining the probabilities of corresponding decay channels one can choose a decay channel at random. The model performs this analysis by the Monte-Carlo method [1].

With a chosen A_0 nucleon system broken up into fragments, the kinetic energies and locations of the fragments in the breakup volume are determined. Next, the expansion of the system due to Coulomb fragment interaction is calculated in the classical way. At the last stage of simulation de-excitation of "hot" fragments is imitated. In this case either the Fermi model [25] or the evaporation model [26,27] is applied. Some complementary details are to be found in [1], where the comparison between model predictions and a number of experimental evidence was made.

According to the model, the nuclear multifragmentation can give information only about the volume and surface energy dependences on temperature. The relative expressions (3) and (4) were proposed ten years ago and, in practice, have not been undergone revision since. But, the availability of two free model parameters - the breakup volume and the volume defining the Coulomb - fragment interaction energy - strongly hamper the extraction of physical information. In particular, it is not inconceivable that the modification to the relation (4), e.g. introducing fragment fractal surface ($S_{AZ} \sim R^\tau_{AZ}, \tau > 2$) can be cancelled by the change of free parameters. Another example is the statistical model [2] taking "cold" fragments production into account. Within the scope of the model under consideration its parameters can be represented by increasing breakup volume (see [1]).

Nevertheless, the model is more justified and physically meaningful than, for instant, the physical concepts of the percolation model. With transport models, the situation becomes more complicated because the multifragmentation characteristics are dictated by the criterion of nucleon joining into "cluster-fragment". The transport model calculations necessitates considerable computatinal effort. At high energies the transport models (except the cascade model) are practically not in use. Therefore, at high energies, it is a good idea to invoke the statistical model to give the broad outlines of multifragmentation and the models approved at high energies to describe the fast stage of reactions (FRITIOF [28], VENUS 29], RQMD [21], HIJING [30] and so on).

3.2 Calculation of residual characteristics (The Regge-model of the fast stage of interactions)

As noted above, the statistical model of multifragmentation contains the assumption of nuclear residuals ensemble with specified features (mass, charge, the excitation energy). The ensemble can be created by simulating the fast stage of reactions in the framework of dynamical models. VENUS model [29] is unsuitable at our energies. As shown in [20], the cascade model considerably overestimates the yield of fast protons (g-particles), i.e. overpredicts the target breakup in interactions of gold nuclei in photoemulsion. However, modified FRITIOF [20] and RQMD [31] give satisfactory results on the yield of g-particles. RQMD model has found application in the description of nuclear multifragmentation quite recently [22]. Taking the sophistication of the model into account, we invoked the simplest phenomenological approach [23] used in the modified FRITIOF program code [20].

The model [23] suggests that with hadron-nucleus interactions each of the interactions of the incident hadron with nucleons of a target nucleus initiates a cascade of Regge exchanges (see Fig.1). The Regge exchange amplitudes are taken in the ordinary Gaussian form. The dependence on nucleon longitudinal coordinates is disregarded, as in the Glauber approximation. It is perceived that all the nucleons involved in the Regge-cascade leave the nucleus.

To clarify the physical content of the model, let us turn to [32], where the elastic NN-scattering amplitude and the repulsive part of NN-potential were found in the scope of the quark-gluon approach. Proposed in [32] was that in the elastic NN-scattering the gluon exchange between quarks of colliding nucleons and further quark exchange between nucleons occur (see Fig.2.). From the Regge approach standpoint, such a process corresponds to the one non-vacuum Regeon exchange between nucleons.

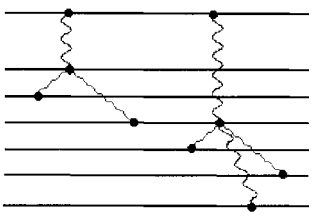

Fig. 1. Hadron-nucleus interaction diagram in the Regge approach. *Straight line* are nucleons, *wavy lines* are Regge exchanges

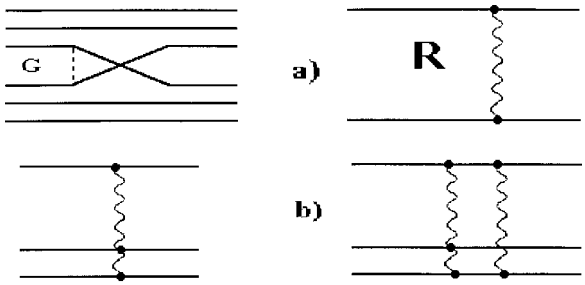

Fig. 2. a Elastic NN-scattering diagram in the quark-gluon approach and corresponding Regge-diagram. **b** Plausible diagrams for interactions of a hadron with two nuclear nucleons

The interaction of the incident hadron with two nucleons apparently may be described by more complicated diagrams, Fig.2b. They can be related to Regge diagrams. Thus far, no consideration has been given to this sort of diagrams.

The Regge description of cascade interactions usually requires that the so-called enhanced diagrams containing the vertices of Regeon interactions be considered. The constants of these vertices are poorly understood. The methods of enhanced diagram contributions calculation are not sufficiently advanced. In view of this, a quantitative description of cascade interactions is in reality absent in the Regge approach.

Quark-gluon view of the process allows another way of looking at the problems of the cascade interaction theory. The calculations of the cascade interaction amplitudes in the framework of the quark-gluon approach is an extremely stubborn mathematical problem. However the relative simplicity of Regge diagrams can help to calculate their contributions. In this context, we take the evidence of [23] as the first step towards the line of investigation.

In other words, we believe that quark-gluon exchanges between nucleons of a nucleus are initiated by collisions of the incident nucleon with nucleons of a nucleus. The nucleons taking part into exchanges leave nucleus, i.e. knocked out. To make allowance for the cascade interactions of knocked-out nucleons is to take more complicated diagrams into consideration. The algorithm proposed in [23] and approved in [20] makes possible listing exchange diagrams.

In the case of nucleus-nucleus interaction we consider that two colliding nuclei each initiate quark-gluon exchanges. The probabilities for the nucleon collisions are given in terms of Glauber expressions [33].

In line with these considerations, the algorithm for residual characteristics calculation was formulated as:

1. Nucleon coordinates of colliding nuclei (x, y, z) and (x', y', z') for the projectile and target respectively were simulated according to the Saxon-Woods distribution. z-axis was directed along the collision axis.
2. The impact parameter is simulated (see [34]).
3. At a given impact parameter, colliding, "wounded" nucleons of nuclei were identified (see [34]).
4. For each "wounded" nucleon i and each spectator nucleon j of the incident nucleus, say, $b_{i,j} = (x_i - x_j)^2 + (y_i - y_j)^2$ was found.
5. The spectator nucleon j was injected into the array of "wounded" nucleons with the probability of $W = C_{nd} \cdot e^{-b_{ij}^2/{r_c}^2}$, $C_{nd} = 0.28; r_c = 1\ fm$. If the number of in-

jected nucleons-participants was no zero, then recipes 4 and 5 were repeated but only for the newly injected participants, otherwise, recipe 6 was carried out.

6. The number of spectator nucleons (A) and the sum of all charges (Z) are determined. These quantities were identified with the mass number and charge a nuclear residual. The kinematic characteristics of nuclear residuals were determined according to the recipe given in [20].

To calculate the excitation energy of nuclear residuals, we took the results of [3] (see Fig.4 in [3]) and parametrized them by:

$$\epsilon^* = 10.5A\left(\frac{A_0 - A}{A_0}\right)^{0.75} \quad (MeV), \quad A_0 = 197.$$

The Glauber AA-cross-sections and the impact parameter distributions call for quantitative features of NN-collision: the total cross-section (σ_{NN}^{tot}), the slope of differential elastic NN-scattering cross-section (B_{NN}^{el}) and the real-to-imaginary elastic NN-scattering ratio at zero-momentum transfer (ρ_{NN}). These values was taken from the compilation [35] for energy 10.6 GeV/nucleon. For 600 MeV/nucleon, the following effective values were in use: σ_{NN}^{tot} = 39 mb, B_{NN}^{ee} = 3.1 $(Gev/c)^2$, ρ_{NN} = 0.2.

The calculation of residuals and the statistical model of multifragmentation allowed the global simulation to be made of gold-emulsion interactions at 10.6 A GeV. The features of produced particles were discussed [20]. The quantitative features of multifragmentation deduced from the present calculations will be given below. In the subsequent discussion we will refer to this approach as the combined model.

First of all "the capability" of the model has been illustrated by the results of the ALADIN collaboration. The description of the basic characteristics for the multifragment decay of Au nuclei at 600 MeV/n has been achieved by fitting the parameter C_{nd} alone: C_{nd} = 0.2. Figure 3a shows Z_{b3}-distributions (in the absolute normalization). As seen, there is a observed peak at large Z_{b3} resulting from neglecting the particular experimental conditions of the ALADIN detectors [6]. At small Z_{b3} the model underestimates the experimental cross-sections. We consider this may be attributed to the target fragments disregarded in the processes with weak excitation of projectile nuclei.

Figure 3b presents the evolution of the mean multiplicity of IMFs as a function of Z_{b3}. The reproduction of this dependence as well as other correlation characteristics studied but not adduced in this study is quite satisfactory. On the whole, we have every reason to point out the remarkable similarities between our results and the prediction of model calculations for multifragment decay of Au nuclei at 600 MeV/nucleon.

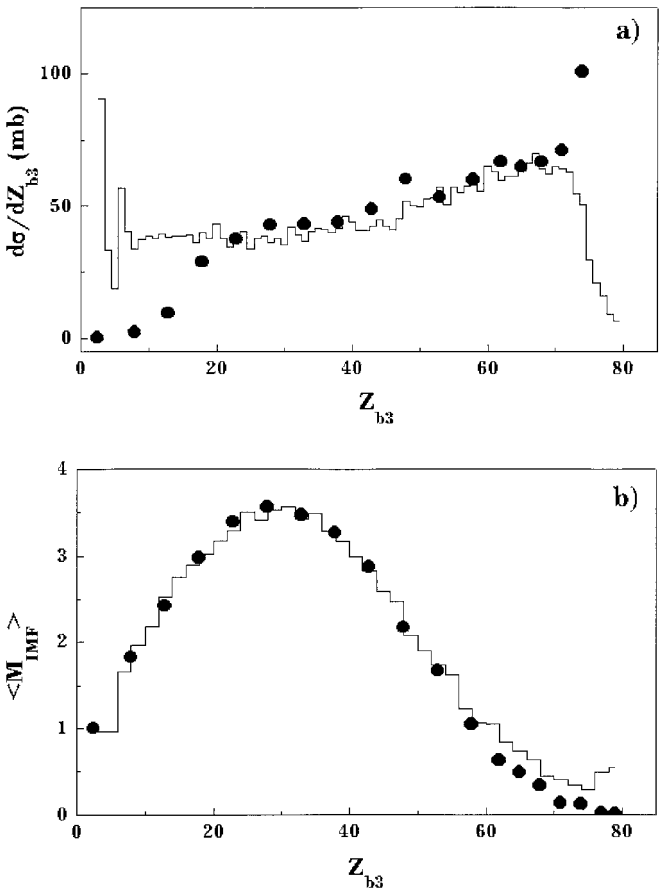

Fig. 3. Z_{b3} distribution and the IMF multiplicity dependence on Z_{b3}. *Histogram* - experimental data points [3], *circles* - calculation

4 Frequency characteristics in interactions of Au with emulsion nuclei

4.1 "Bound" charge distributions

If it is granted that the production of thermalized nuclear residuals takes place, the main characteristics of interactions must be the nuclear residuals distributions of the fragment mass, charge, excitation energy and kinematical variables. Unobservability of neutrons in emulsion experiments, difficulties encountered in the determination of nuclear sizes and in measuring longitudinal fragment momenta impose the restriction on the present investigation. In this context, the charge distributions of nuclear residuals hold an important place being a tool for the study of multifragmentation. In so doing, it is necessary to have in mind that protons participating in the fast stage of interaction and those producing during the multifragmentation are indistinguishable. As the model estimates show, among observed singly charged fragments whose average multiplicity is 8.07 ± 0.16 the fraction of the fragments producing during the nuclear multifragmentation does not exceed 50%. The charge bound in multiply charged fragments one can therefore consider as a measure of the charge of thermalized nuclear residuals.

Figure 4a giving an illustration of the evolution of Z_{bound} after the fast stage termination shows a comparison of the measured Z_{bound} distribution with the results of the model simulation (Z_{bound} is the sum of all fragment charges with $Z \geq 2$). Experimental and predicted distributions for Au + Em interactions were normalized to the inelastic cross section (3162 mb) calculated in the scope of the Glauber approximation [34]. From the model distribution two data points corresponding to the cross section at Z_{bound} =78 and 79 were dropped. An allowance was made for the fact that the measured events with hardly charge-changed projectile track were classified as the

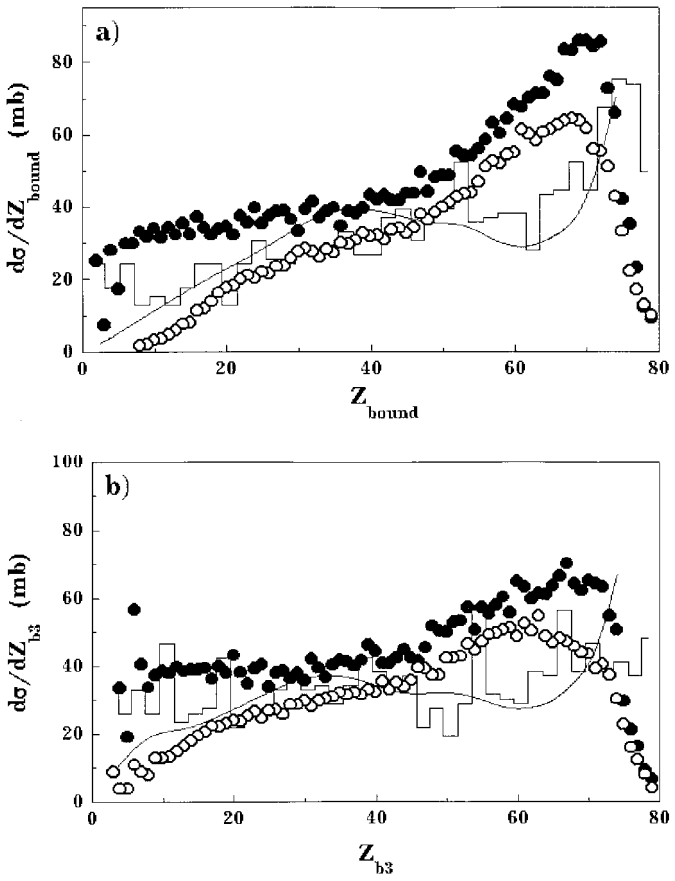

Fig. 4. "Bounds" charge Z_{bound} and Z_{b3} dependencies. Closed and open circles are data of [3]: $Au + Cu$ and $Au + Al$ at 600 A MeV, respectively. *Histograms* - the present results: $Au + Em$ at 10,7 A GeV. *Solid curves* - the combined model predictions

events of electromagnetic dissociation and were consequently excluded from the ensemble under study. Such events could also be missed in scanning.

According to the calculations, the average mass of targets taking part in interactions is 46.8. So we have considered that a comparison between our findings and interactions of Au+Al and Au+Cu at 600 A MeV (the data of the ALADIN collaboration) [3,6] is worthwhile. As illustrated in figure, the observed Au - breakup is slightly stronger at high than at intermediate energies: Au+Em data points lie lower than those corresponding at intermediate energies in the $50 \leq Z_{bound} \leq 70$ range. At $Z_{bound} < 50$ all the data points are in reasonable agreement, which speaks for some universality of strong breakup.

The Z_{bound} and Z_{b3} distributions, as the calculations indicate, are little sensitive to the excitation energy of nuclear residuals. So, 10% decrease in the excitation energy of nuclei permitting the IMFs description (see below) has little effect on the Z_{bound} distributions. In turn, they do depend strongly on the mechanism of nuclear breakup at the fast stage. The value of the parameter C_{nd} = 0.2 such that the description of the ALADIN evidence is achieved fails to lead to expected results at high energy. However, at C_{nd} = 0.35 the multiplicity distributions of grey tracks is fairly well reproduced [20] but the degree of Au nuclei disintegration is rather overestimated. For further calculations we chose the value C_{nd} = 0.28. The change in this parameter in transition from 600 A MeV to 10.6 A GeV, to our opinion, reflects the fact that cascade interactions of produced particles increases in importance. The calculations also give that the average number of singly charged particles produced in multifragmentation does not exceed 3. Hence Z_{bound} is a good charge estimation of nuclear residuals.

Similar conclusions can be drawn by analyzing the Z_{b3}-distribution in Fig.4b (Z_{b3}-the sum of all charges with $Z \geq 3$). Observed here is a better than in the foregoing case agreement between the predictions and experimental data on Au + Em-interactions. This does not mean that the value of Z_{b3} more adequately depicts the charges of nuclear residual than Z_{bound}. The fact is that the model underpredicts two charged fragment multiplicity, i.e. overestimates the values of Z_{b3}. So, if it is believed that fragments with Z = 2 may be emitted both at the fast stage and prior to multifragmentation (these processes are not considered in our approach), then the calculated curve should be left shifted, which has no significant effect on describing data but is capable of eliminating the disagreement between Fig.4a. and 4b.

In total, we consider that the combined model satisfactorily reproduces the distributions of Z_{bound} and Z_{b3} and provides a correct relation between interactions with light and with heavy emulsion components at C_{nd}=0.28. Note, that the description of data at high energies is first obtained by adjusting only one parameter: C_{nd}.

4.2 The multiplicity distributions of fragments

The conjectured statistical character of the breakup of thermalized nuclei must give rise to fluctuations of fragment multiplicities. The observed fluctuations are due to both this reason and the fluctuation of the number of nucleons knocked out at the first stage of interaction and, in addition, a complex emulsion composition[3]. Because of this, a qualitative description of multiplicity distributions of fragments within the framework of the combined model seems reasonable.

Experimental and calculated singly charged multiplicity distributions are plotted in Fig.5a. There in, the multiplicity distribution of singly charged multifragmentation particles is shown . The multiplicity of multifragmentation particles, as is seen, fluctuates within a narrow range (see the dotted curve). Yet, the main contribution to single charged multiplicity is associated with the processes of the first stage. Hence, further improvements in the above distribution must have to do with perfecting the model of the fast interaction stage.

Figure 5b demonstrates the IMFs distribution. One can see that the production of the fragments under discussion is characteristic of 60% of the interactions, i.e. the nuclear multifragmentation is the dominating decay mode at high energies. The model fairly correctly reproduces the experimental distribution, with increased multiplicity pulling the model and experimental points together. Striking disagreement between the experiment and the model is found at n_{IMF}=1 and 2. Instantaneous the total multiplicity distribution of multiply charged fragments ($Z_F > 2$) is fairly well represented by the model, Fig.5c. A dramatic discrepancy is apparent only for the events of "total" dissociation of the nuclei ($n_{Z>2}$ = 0) into singly and two charged fragments.

[3] Note, photoemulsion is the composition of the following nuclei: $H(37,6\%)$, $C(17,8\%)$, $O(4,7\%)$, $N(13,6\%)$, $Br(13,1\%)$ and $Ag(13,1\%)$

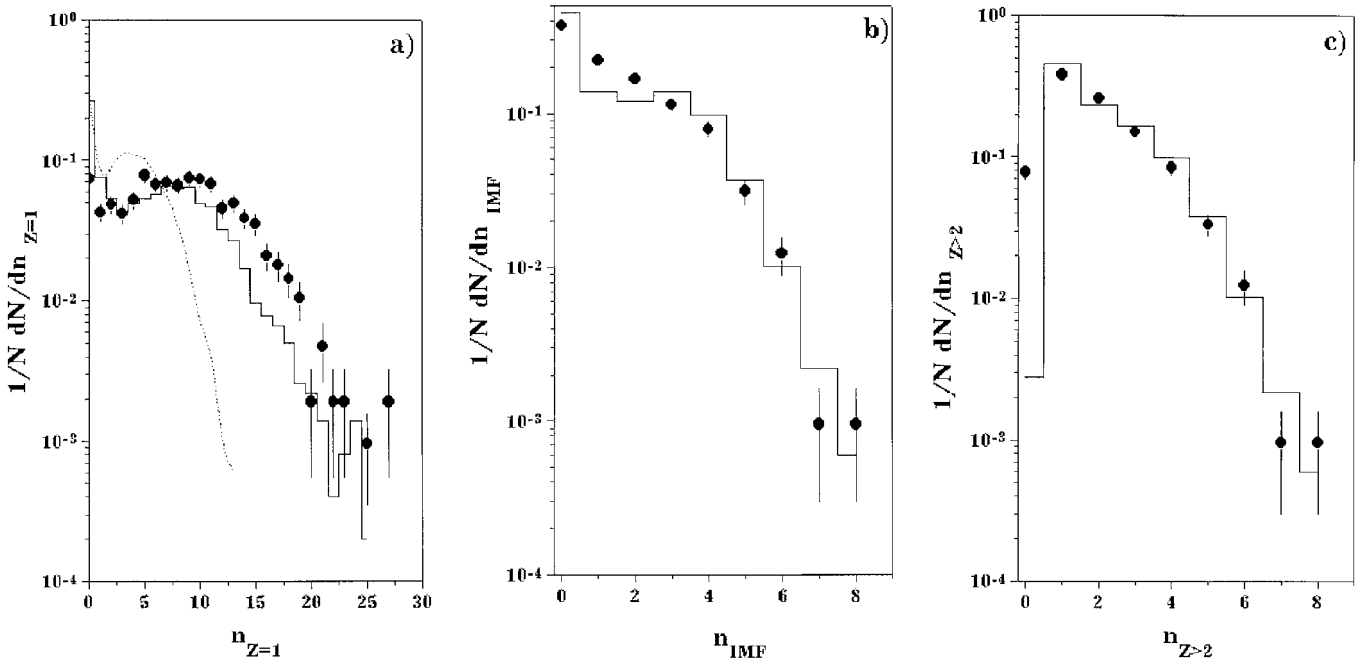

Fig. 5. a Singly charged fragment multiplicity distribution, **b** IMFs multiplicity distributions, **c** Distribution of multiply charged fragments with $Z_F \geq 3$. *Circles* - experimental data points, *histograms* - the results of the combined model. *Dotted curve* is the multiplicity distribution of singly charged fragments producing at the multifragmentation stage of gold nucleus residuals only

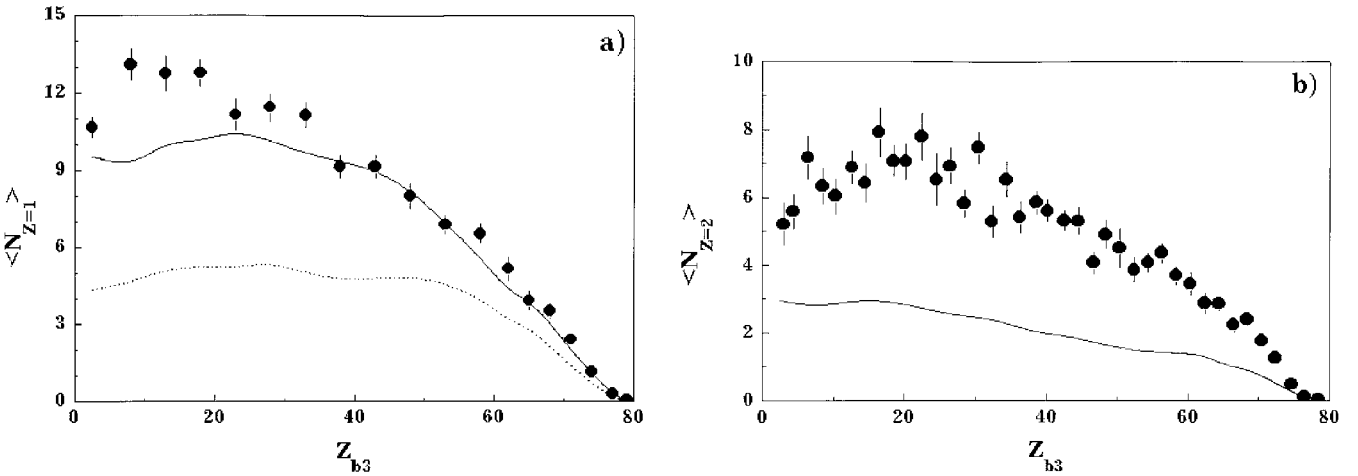

Fig. 6. The average multiplicity of singly charged fragments (Fig. a) and the average multiplicity of two charged fragments (Fig. b) as a function of Z_{b3}. *Circles* - experimental data points. *Solid curves* - predictions according to the combined model. *Dotted curve* - the contribution of singly charged fragments created during the nuclear fragmentation (Fig. a)

Some model overestimation takes place at $n_{Z>2}$ = 1. The events with $n_{Z>2}$ = 1 may be attributed to collisions with large Z_0 (peripheral collisions) and to the most violent collisions with small Z_0 (total dissociation). To find out the reproducibility of the model, of interest is the consideration of fragment multiplicity at small and large Z_{bound} (Z_{b3}).

4.3 The dependence of fragment multiplicity on Z_{bound} and Z_{b3}

Figure 6a shows the dependence of the singly charged multiplicity on Z_{b3} together with the predictions with and with no particles involved in the fast stage of interaction (solid and dotted curves, respectively). According to the model the fraction of the singly charged fragments produced at the multifragmentation stage does not exceed 50%. The features of singly charged fragments selected by conventional emulsion techniques may therefore be distorted well by multiparticle production at the fast stage of interaction.

At $Z_{b3} > 30$, a reasonably good description of experimental dependencies stands out. The combined model does underestimate the singly charged multiplicity at small Z_{b3}. Increased multiplicity can be reached by increasing the value of the parameter C_{nd}, but, in doing so, the description of the Z_{bound}, Z_{b3} distributions becomes worse. Provided the parameter C_{nd} be unchangeable, the singly charged fragment multiplicity can be increased by a more accurate characteriza-

tion of ejected nucleons (see [20]). It is not improbable that it can also be achieved at the expense of modification of the multifragmentation model or a closer consideration of a stronger breaking of nuclei into fragments. Obviously, this problem needs further investigation.

To give an account of the yield of two charged fragments is much simpler. According to Fig.6b, the model greatly underestimates the two charged fragment multiplicity among which ^4He nuclei dominate. We consider that this model disadvantage may be due to choosing fragment mass by the distribution rejecting the extra yield of two and three charged fragments (for details see [1],p.159), on the one hand, and neglecting possible knocking out of fragments with Z = 2 at the fast stage, on the other hand. As an argument for the second hypotheses, we dealt with the transverse momentum distribution of the two charged fragments, which, as deduced from the experiment, has a complicated structure [36-38]. In practice the calculations fail to give a structure of the distribution. Furthermore, we would like to call reader's attention to the similarity of Fig.6a and 6b. Without recourse to considering nucleons ejected at the first interaction stage, these distributions would be identical if the data of Fig.6a were multiplied by corresponding scale factor $\sim$ 0.7. This fact is unexpected and deserves further investigation[4].

Let us turn to the IMFs multiplicity ($3 \leq Z_F \leq 30$). As pointed before [3], the mean IMFs multiplicity ($< n_{IMF} >$) as a function of Z_{bound} or Z_{b3} is essentially independent of target mass in interactions of 600 MeV/n gold nuclei with various nuclei. Figure 7 presents the evolution of the mean IMFs multiplicity as a function of Z_{bound}, Z_{b3} other than that obtained by the ALADIN-group [3].

The data similar to our findings of Fig.7a have been reported by KLMM-collaboration [16] and in work [15]. The authors have pointed out that, at $Z_{bound} > 40$, the data agree well. However, it is seen from Fig.7b that, at intermediate and high energies, the discrepancy between experimental results takes place over the whole interval of Z_{b3}. Our statistics are not reach enough to give conclusive results. Nevertheless, it is believed that at high energies the common features suppressed at intermediate energies become to show itself.

The discrepancy between data at intermediate and high energies (like in Fig.7b) can be obtained over the whole interval of Z_{bound} if it is considered that about 50% of α-particles are registrated in ALADIN-experiment [3]. The histogram in Fig.7a shows the result of our calculations obtained from random 50% allowance for α-particles identified in emulsion. It should be remembered that in the ALADIN experiment [15,16] (used in this work for comparison) the fragments with Z = 2 are registrated differently than in the emulsion experiment. This circumstance is responsible for the existing disagreement between data cited and our results.

Let us proceed to the theoretical description of the data. The combined model fairly well reproduces the features in question at intermediate energies and suggests they to be unchanged at high energies (see solid curves in Fig.7). The model predictions and our results can come closer together (see dotted curves in Fig.7) if assuming that at high energies nuclear

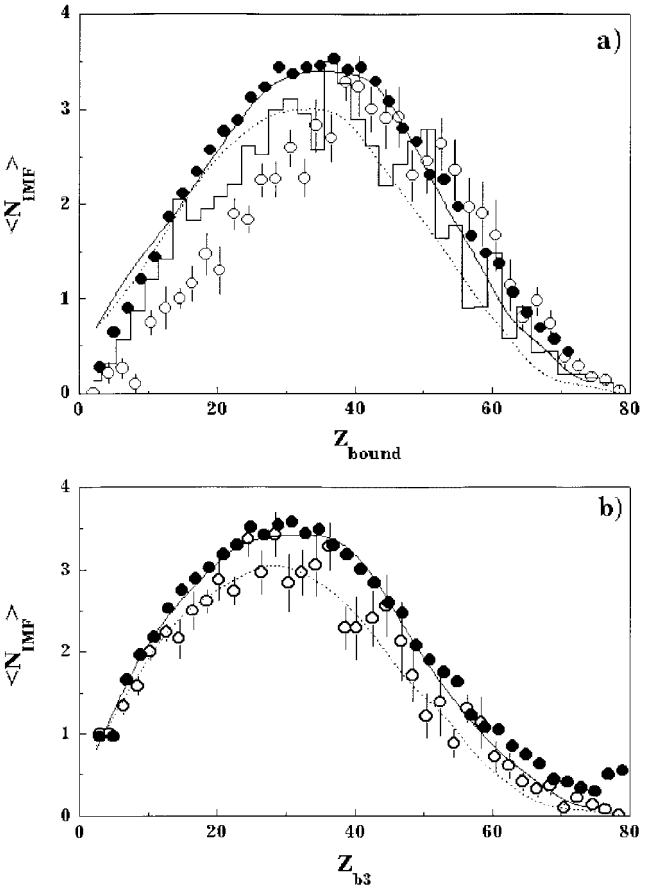

Fig. 7. The average multiplicity of IMFs as a function of Z_{bound} and Z_{b3}, (Fig. a and b respectively). *Closed circles* are data [3] of Au + Cu at 600 A MeV. *Open circles* are our data. *Histogram* (Fig. a) is the experimental data obtained with allowance for 50 % efficiency of the registration of fragments with Z = 2 on the ALADIN setup. *Solid* curves (on Fig. a and b) - the results of the combined model. *Dotted curves* - similar calculations with the excitation energy of nuclei reduced by 10 %

residuals acquire slightly lesser excitation energy than at intermediate.

ε^* = $9.45A_{res}(A_{res} - N_{ej})^{0.75}$.

The average charge distribution of the heaviest fragment in an event, one would think, does indeed favor a lesser excitation energy, Fig.8a. The good agreement between $< A_{12} >$ and $< A_{23} >$ within the experimental errors at high and intermediate energies (see the definition in [3]) indicates, in turn, that at high energies these fragments, on average, are heavier. As it follows from figures, the combined model with the reduced excitation energy reasonably well represents the experimental results.

An alternative explanation for these special features of our data may also be offered. The work [14] dealt with an effect of nuclear residual angular momentum on characteristics of nuclear multifragmentation. It has been shown that the angular momentum enhancement results in decreasing IMFs multiplicity and increasing the average charge of the heaviest fragment, what is consistent with our observation. Thus, the average angular momentum of nuclear residuals may be assumed to enhance greatly in transition from intermediate to high energies.

[4] As a theme for meditation we remind the work of L.Dakhno and N.Nikolaev [39] on 12%-mixture of 12-quark bag state in the ground state of ^4He. Also, on a plausible explanation for EMC-effect assuming such bags in the heavy nuclei [40]

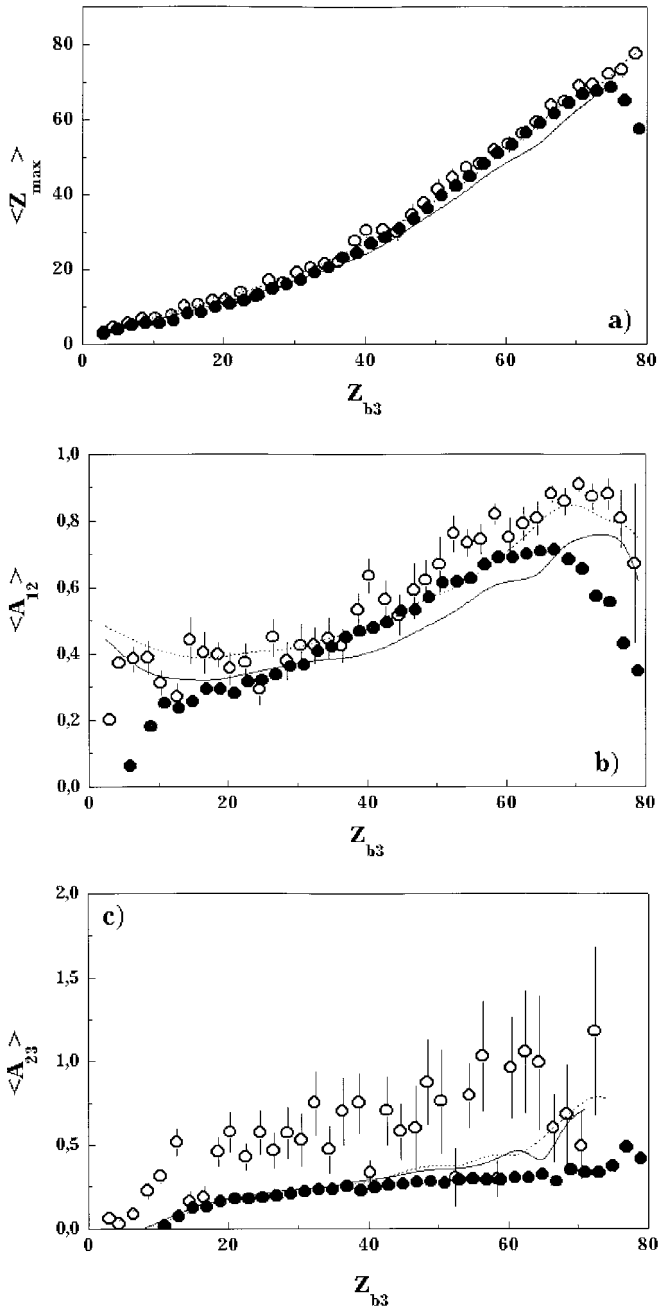

Fig. 8. The average charge of the largest fragment in the event and average asymmetry coefficients A_{12} and A_{23} as a function Z_{b3}. *Closed points* - the data of ALADIN [3], *open points* - our data. *Solid curves* - the combined model predictions. *Dotted curves* - calculations with the reduced excitation energy

To decide between the two hypothesis, it is necessary to examine more specifically the data.

5 Search for possible dynamical effects

The model of multifragmentation used here suggests a statistical isotropic decay of thermalized nuclear residuals at rest. Asymmetrically emitted fragments or a "memory" of the stage of forming nuclear residuals, i.e. some strong correlations

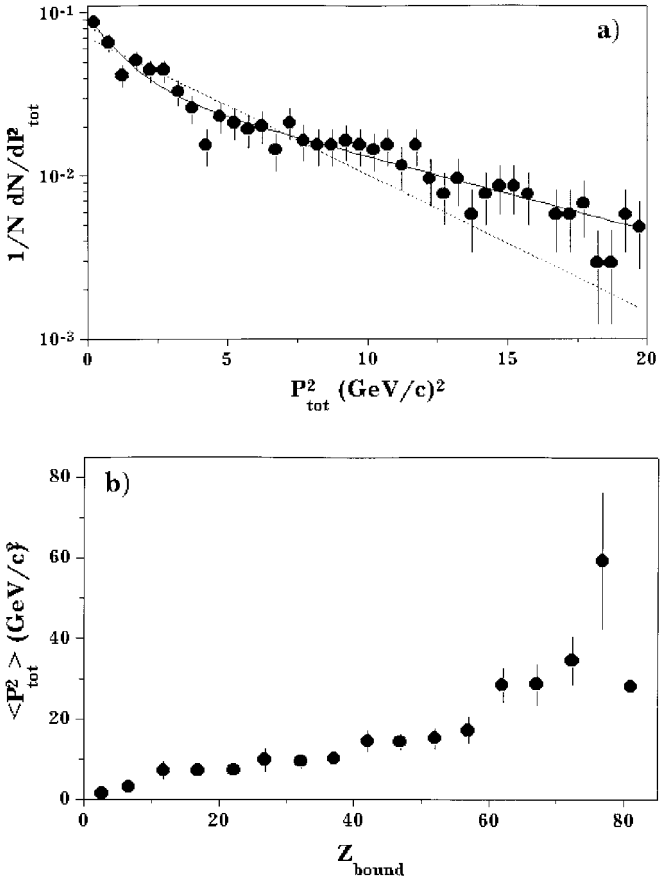

Fig. 9. a The distribution of the total transverse momentum transferred to the system of spectator fragments. *Solid curve* - the approximation with two exponential. *Dotted curve* - the approximation with one exponential. **b** The mean transverse momentum squared versus Z_{bound}

between fragment characteristics of resuduals and kinematic characteristics in the lab. frame may therefore hardly be expected.

To analyze such correlations, it is necessary to make a translation to the nuclear residuals rest frame as fragment characteristics may be distorted by the moving residual nucleus. To do this, we used the following procedure:

1. The transverse momenta of fragments with $Z_F \geq 2$ were determined (see Sect. 2);
2. The total transverse momentum of fragments and the velocity of a spectator group of fragments was found

$$\mathbf{P}_{tot} = \sum_F \mathbf{p}_F, \qquad \mathbf{V} = \mathbf{P}_{tot}/2m_N \sum_F Z_F.$$

   Here m_N - the mass of the nucleon.
3. The fragment momentum in the nuclear residual rest frame is defined as

$$\mathbf{p}\prime_F = \mathbf{p}_F - 2m_N Z_F \mathbf{V},$$

   what corresponds to the Gallilean non-relativistic transformation into the moving frame.

Of interest is both the fluctuations of $\mid \mathbf{P}_{tot} \mid$ and the dependence of $<\mid \mathbf{P}_{tot} \mid^2>$ on the fragment mass, on the "bound"

charge. Figure 9a gives the $\mid \mathbf{P}_{tot} \mid^2$ -distribution in all interactions. This figure points clearly to the presence of the large momentum, i.e. the system of spectator fragments can gain a relatively large transverse momentum. In this connection, the translation to the fragmenting nucleus rest frame seems imperative.

Attempts to find a good fit (the only exponential - the dotted curve) has met with only limited success. This send us in search of a curve which is the sum of, at least, two exponentials with different slopes (see the solid curve). The similar situation has taken place when discussing the transverse distributions of two-charged fragments [36-38]. The data obtained were then interpreted as some evidence for several sources of α-emission with different momenta P_t. The present data can be regarded as some evidence for two mechanisms of transferring a transverse momentum to the system of spectator fragments.

Figure 9b shows $<\mid \mathbf{P}_{tot} \mid^2>$ as a function of Z_{bound}, which also gives indication of large momentum transfers. Not counting the Coulomb interaction of nuclei, there would be expected to be a parabolic dependence of $<\mid \mathbf{P}_{tot} \mid^2>$. According to Feshbach's statistical multifragmentation model [41], much the same behavior is observed for $Z_{bound} < 40$. At large Z_{bound}, we think that the Coulomb nuclear interactions come to play a noticeable role.

Clearly the dependences under study are governed by the dynamics of the fast stage and the used model of multifragmentation fails to describe the features unique to it. The model does suggest the lack of correlations between fragment characteristics in the residual rest frame and dynamical variables like P_{tot}.

5.1 Azimuthal correlations

The simplest correlation characteristic of the interaction is the φ-distribution between the fragment transverse momentum $\mathbf{p}'_i$ in the fragmenting nucleus rest frame and nuclear residual transfer momentum.

$$\varphi = arcCos[(\mathbf{p}\prime_i \bullet \mathbf{P}_{tot})/ \mid \mathbf{p}'_i \mid\mid \mathbf{P}_{tot} \mid].$$

The histograms on Fig.10 present the φ-distributions for different fragments. As observed in Fig.10, the anysotropy is hidden from view in the angular distribution of all fragments, which results from the imposition of fragment characteristics. Two-charged fragments, c.f. figure, are emitted predominantly towards the transfer transverse momentum. Multiply charged fragments as well as fragments with the largest charge in an event are emitted in the opposite direction. The regularities can be understood by assuming that the transfer transverse momentum, P_{tot}, does not lie in the plane containing the projectile momentum and the center of target. This is possible if the nuclei are not hard spheres.

The combined model does not suggest any anysotropy of the decay. Even so, the fragment momenta conversion to the residual rest frame and the assumption of the same number of protons and neutrons in fragments give rise to some decay anysotropy, c.f. Table 1, where the average cosines of emission angles of fragments, ($< Cos(\varphi) >$), are listed. It follows from Table 1 that the model fails to reproduce the anysotropy of the heaviest fragments.

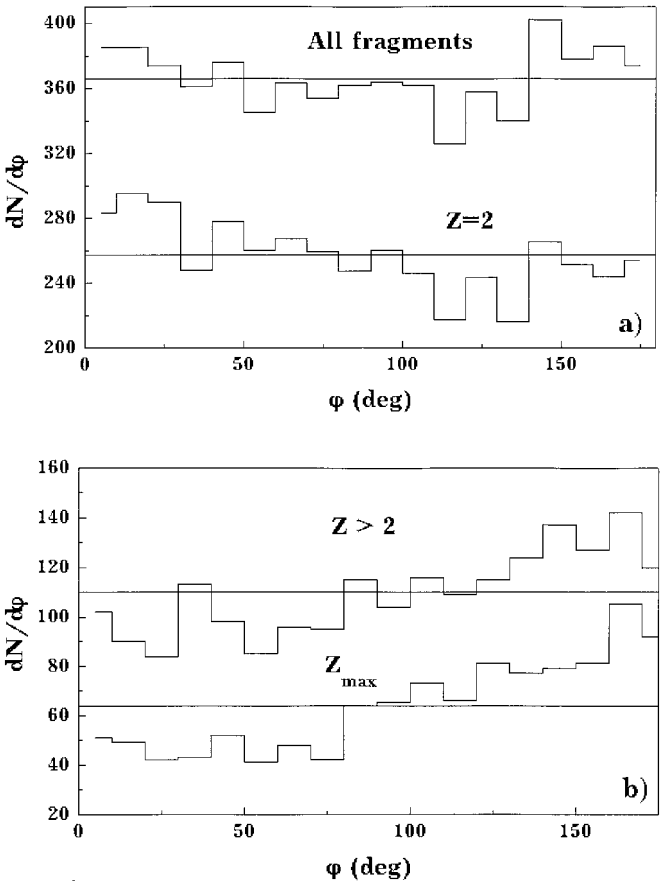

Fig. 10. Angular distributions of all fragments and fragments with Z = 2 (Fig. a), multiply charged fragments with $Z_F > 2$ and the heaviest fragments (Fig. b). The emission is taken with respect to the direction of the total transfer momentum in the fragmenting nucleus rest system. *Straight lines* are isotropic distributions

Another anysotropy indicator of fragment emission is the azimuthal angle difference distribution in the residual rest frame. The quantitative assessment of the decay anisotropy provides the coefficient of azimuthal asymmetry defined as

$$A = \frac{N_{pair}(\Delta\varphi > 90^o) - N_{pair}(\Delta\varphi \leq 90^o)}{N_{pair}(\Delta\varphi > 90^o) + N_{pair}(\Delta\varphi \leq 90^o)},$$

where N_{pair} ($\Delta\varphi > 90^o$) - the number of fragment pairs having the angle difference $\Delta\varphi > 90^o$ and so on.

Table 1. The average cosine of fragment angels with respect to the direction of the momentum transferred to the nucleus residual in the rest frame of the fragmenting nucleus

	Exp.	Model
All fragments	0.0006 $\pm$ 0.0088	0.0273
Fragments with Z = 2	0.0378 $\pm$ 0.0105	0.0723
IMF	-0.0777 $\pm$ 0.0182	0.0329
Fragments with ($Z_F \geq 3$)	-0.0868 $\pm$ 0.0160	-0.0700
The heaviest fragments	-0.1867 $\pm$ 0.0206	-0.0973

Table 2. Coefficients of azimuthal anisotropy of fragment emission in the rest frame of the fragmenting nucleus

	All fragments $Z \geq 2$	$\alpha - \alpha$ $Z = 2$	frag. - frag. $Z \geq 3$
$3 \leq Z_{b3} \leq 19$	0.070 ± 0.015	0.038 ± 0.021	0.047 ± 0.078
Model	(0.161)	(0.030)	(0.274)
$20 \leq Z_{b3} \leq 39$	0.025 ± 0.009	0.045 ± 0.022	0.068 ± 0.044
Model	(0.087)	(-0.007)	(0.187)
$40 \leq Z_{b3} \leq 59$	0.078 ± 0.013	0.015 ± 0.031	0.209 ± 0.054
Model	(0.218)	(-0.045)	(0.434)
$60 \leq Z_{b3}$	0.381 ± 0.029	-0.033 ± 0.060	0.541 ± 0.088
Model	(0.652)	(0.051)	(0.706)
All interactions	0.147 ± 0.010	0.037 ± 0.016	0.167 ± 0.037
Model	(0.269)	(-0.002)	(0.378)

Table 2 gives the values of the coefficients for various fragment groups for the events with different Z_{b3}. The two charged fragments are emitted near-isotropically. At the same time, the fragments with $Z_F \geq 3$ are largely given off in opposite directions, the asymmetry coefficient for multiply charged fragments enhancing with increasing Z_{b3} (see column 4 of Table). This may be due to increasing the fraction of events with two fragments for which A=1.

Contrary to the expectations, the asymmetry predicted by the model is greater than observed in the experiment. Since the model takes no account of the nuclear residual rotation, and the fragment emission in Au induced interactions tends to have asymmetry which is lesser than that predicted by the model, we cannot argue in favor of the large angular momentum of nuclear residuals.

5.2 Sphericity analysis of events

It is readily shown that the coefficient of the azimuthal asymmetry in the rest frame of the nuclear residual is close to unity both for events with two fragments and for the events in which one fragment has a large transverse momentum while all the rest have small. In the events with two groups of oppositely emitted particles, for two-jet events, the asymmetry coefficient is close to zero as with isotropic emission of all particles. To study the possible jet-structure of the fragment emission we thus made use of the sphericity analysis.

The sphericity analysis was proposed in [42] and found use in studies of e^+e^--interactions. The most frequently used value is the so-called energy flow tensor

$$T_{\alpha\beta} = \sum_i \frac{1}{2m_i} p_{i,\alpha} p_{j,\alpha}.$$

Here m_i and $\mathbf{p}_i$ - is the mass and the momentum of the i-th fragment, and Greek indices take the values x, y, z. The eigenvalues of the tensor $\lambda_1, \lambda_2, \lambda_3$ are the solutions of the equation

$$\mid T - \lambda I \mid = 0.$$

The value of sphericity is then determined as

$$S = \frac{3}{2} \frac{\lambda_2 + \lambda_3}{\lambda_1 + \lambda_2 + \lambda_3},$$

if the eigenvalues are ordered as $\lambda_1 \geq \lambda_2 \geq \lambda_3$.

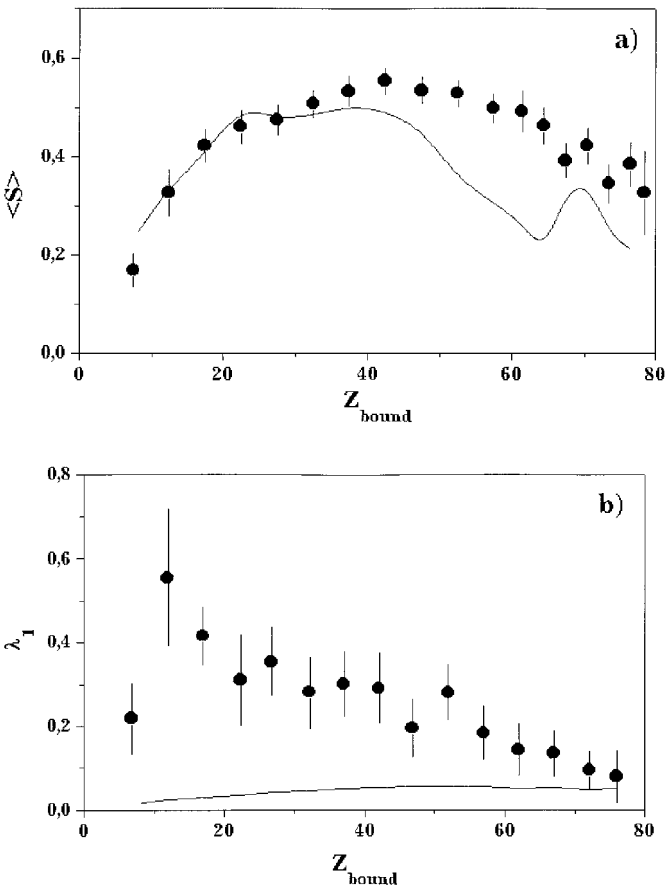

Fig. 11. The average sphericity of events (Fig. a) and the average of the largest eigenvalue of energy flow tensor (Fig. b) as a function of Z_{bound}. *Circles* - experimental data. *Solid curves* - calculations

In the present study, when we use only the transverse momenta of fragments ($\alpha = x, y$), the energy flow tensor has two eigenvalues λ_1 and λ_2. So the sphericity S is of in the form

$$S = 2\frac{\lambda_2}{\lambda_1 + \lambda_2}.$$

The sphericity is certain to depend on both the reference frame and the particle multiplicity. For the mixture of ideal gases in the c.m. frame S is close to unity. In any other moving frame, $S < 1$.

It is also clear that the energy flow tensor can be specified for different particles, e.g. for two and multiply charged fragments. In the case of statistical equilibrium, for various components the mixture spericities must be equal or comparable.

With two particles (even if their mass are unequal) observed in the c.m. frame, $S \equiv 0$. For three or four identical c.m. particles homogeneously filling the accessible phase space, $S \sim 0.5$. Hence, studying the multifragmentation of nuclei, we cannot expect that S will be close to unity.

Plotted in Figure 11a is the average values of S in the events with different Z_{bound} for all available fragments with $Z \geq 2$. In calculating the sphericity we took only the events in which the number of spectator fragments was more or equal 3.

As would be expected, the sphericity tends to zero at small and large Z_{bound}. At $Z_{bound} \sim 40$, the maximum

sphericity is reached all over the fragment system. The model should be noted to reproduce the experimental dependence at $Z_{bound} \leq 40$. At $40 < Z_{bound} \leq 60$ the significant discrepancy between the predictions and experimental data is observed. At $Z > 60$ the model gives some enhancement in spericity. Such a behavior of the predictions can be accounted for the model triggering the evaporation model of de-excitation of nuclei if the excitation energy of a nucleus does not exceed 3 MeV/n [43]. At higher excitation energies the statistical, microcanonical model is applied. The dividing line between the mechanisms of nuclear de-excitation (3 MeV/n) has yet shown sign of being noticed in comparing model calculations and experimental evidence.

On the whole, the model sphericity is somewhat smaller than the experimental. The experimental events are characterized by "good" isotropy of fragment emission.

Of interest is the dependence of eigenvalue of the energy flow tensor λ_1 on Z_{bound}, Fig.11b. Here we find a dramatic discrepancy between the model predictions and experimental results. λ_1 is proportional to the average kinetic energy of fragments. As seen from figure, the average kinetic energy of fragments observed is higher than it is predicted and, consequently, it is worthwhile verifying this observation.

5.3 Transverse momentum dependence of fragments on Z_{bound}

A non-trivial consequence of the model under study is that the kinetic energy of fragments is governed principally by the Coulomb interactions of fragments. As shown in [44], if at the initial stage of nuclear breaking into fragments the average kinetic energy is $\sim$6 MeV, at the final stage it is $\sim$ 20 – 25 MeV by virtue of the Coulomb repulsion of fragments. This is illustrated in Fig. 12, where our estimates of kinetic energies of fragments in the nuclear residual rest frame together with the model calculations are plotted

$$< E >= \frac{3}{2} < \frac{\mathbf{p}_i'^2}{4 Z_F m_N} > \ .$$

As would be expected, the model predicts decreasing in the mean transverse momentum squared with decreasing Z_{bound}. However, there is a rise in $< p_i^2 >$ with decreasing Z_{bound} observed for two charged particles. This is more evident in Fig.12, where the discrepancy between the model predictions and experimental data, like that observed in Fig.11b, is available. Unfortunately, the limited statistics of our data allow only the tendency for fragments with $Z_F \geq 3$ to be seen. We believe that more realistic evidence can be obtained by "electronic" experiments.

The average kinetic energies of fragments obtained experimentally and theoretically are listed in Table 3. The disagreement between results and predictions is neatly traced.

The enhancement or permanence of the mean transverse momentum squared as the size of residual nucleus decreases can be caused, at least, two causes - the large angular momentum transferred to nuclear residual [14] or the radial flow of fragments. The angular asymmetry of the decay was analyzed in the previous Chapter. The events have no well-marked anisotropy. The presence of non-thermal, collective component in the energy of fragments remains to be presumed.

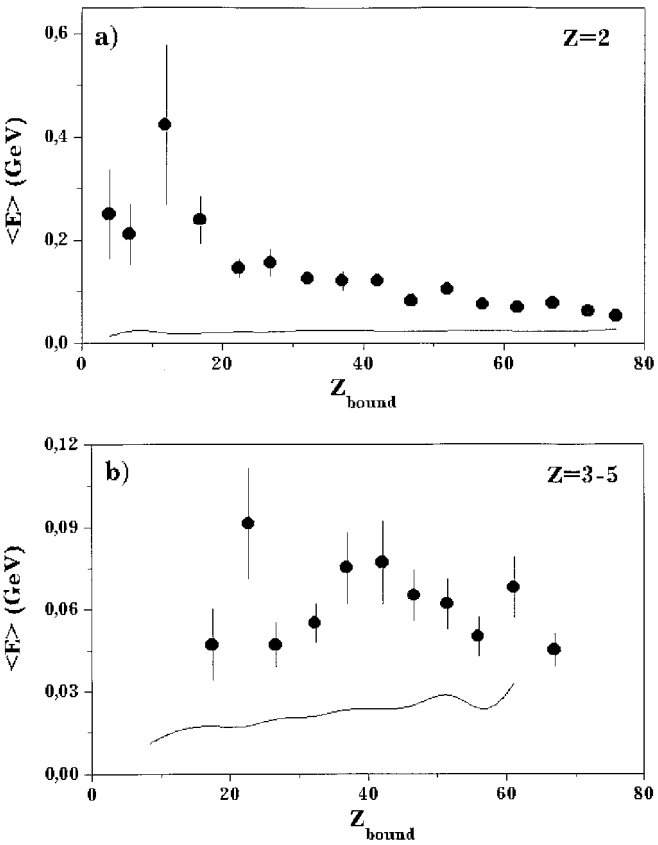

Fig. 12. The average kinetic energies of two-charged fragments with Z_F = 3 – 5 as a function of Z_{bound}. *Circles* - experiment. *Solid curves* - calculations

Table 3. Estimates of the average kinetic energies of fragments in the rest frame of the fragmenting nucleus

Z	Exp.	Model
2	67.3 ± 3.0	16.7
3, 4	47.5 ± 2.0	17.4
5, 6	54.2 ± 3.1	19.2
7, 8	52.5 ± 3.2	20.8

The average fragment energies, as noted in experiments at low and intermediate energies[13], is proportional to their sizes. This fact was interpreted as the availability of a radial flow of fragments originating from the expansion of strongly compressible nuclear matter. We cannot assert that all the interaction under study are central. In addition, with our present statistics, it is not possible to draw a conclusion that energies of fragments and their sizes are proportional to each other, while such a tend is available. Thus we consider our data on kinetic energies as evidence for existing the radial flow in peripheral collisions. Clearly the initiation of the radial flow is one more dynamical process adding complexity to the sophisticated enough picture of the dynamical evolution and inviting further investigation.

6 Summary

Experimental data on multifragmentation of 10.6 A GeV Au nuclei in interactions with nuclear photoemulsion are pre-

sented. Systematic comparison is made of the results obtained with those of the ALADIN collaboration (Au at 600 A MeV). A systematic discrepancy between the two sets of data is found.

It is shown that allowance for the registration efficiency of two charged fragments on the ALADIN setup is needed to compare Au-fragmentation data at high and intermediate energies. Considering the registration efficiency of two charged fragments one can conclude unambiguously that the IMFs multiplicity at high energies is smaller as compared with that observed at intermediate energies. On the average, at high energies the charge of the heaviest fragment in an event is larger than at intermediate.

These features of multifragmentation at high energy may be due to collective effects: the large angular momentum of nuclear residuals or the radial flow of fragments. Evidence of the large angular momentum is not yet found: the events are appreciably characterized by azimuthal symmetry. Kinetic energies of fragments do indeed suggest that there is a radial flow of spectator fragments.

The estimation method of mass, charge and excitation energy of gold nucleus residuals creating in nucleus-nucleus interactions at high and intermediate energies is proposed. It allows the main features (except the radial flow) of multifragmentation in the framework of the statistical model of multifragmentation [1] to be represented.

The financial support from the Australian Research Council, the National Natural Science Foundation of China, the Foundation of the State Education Commission of China, the Grant Agency for Science at the Ministry of Education of Slovac Republic and the Slovac Academy of Sciences, the German Federal Minister of Research and Technology, the German Found of DLR, the German Academic Exchange Service (DAAD), the University Grants Commission and the Department of Science and Technology of the Government of India, the Korean Science and Engineering Foundation, the Romanian Ministry of Research and Technology and the National Science Foundation, the Russian Foundation of Fundamental Research, the Swedish Natural Science Research Council, the United States Department of Energy and National Science Foundation and the Foundation of Fundamental Research of Academy of Sciences of Uzbekistan, are cordially and gratefully acknowledged.

References

1. J.P. Bondorf, A.S. Botvina, A.S. Iljinov, I.N. Mishustin, K. Sneppen, Phys. Rep., **257**, 134 (1995)
2. D.H.E. Gross, Rep. Prog. Phys., **53**, 605 (1990)
3. A.S. Botvina et al., Nucl. Phys. A, **584**, 737 (1995)
4. J. Hubele et al., Zeit. fur Phys. A, **340**, 263 (1991)
5. J. Hubele et al., Phys. Rev. C, **46**, R1577 (1992)
6. P. Kreutz et al., Nucl. Phys. A, **556**, 672 (1993)
7. S.M. Kiselev, Phys. Lett. B, **240**, 23 (1990); Nucl. Phys. A, **579**, 643 (1994)
8. J. Aichelin, Phys. Rep., **202**, 233 (1991)
9. T.L. Hill, "Statistical Mechanics. Principles and Selected Applications", McGraw-Hill Book Company, New-Yourk - Toronto - London, 1956
10. C.O. Dorso, P.E. Balonga, Phys. Rev. C, **50**, 991 (1994); P.E. Balonga, C.O. Dorso, Phys. Rev. C, **52**, 915 (1995); A. Aranda, C.O. Dorso, V. Furci, J. A. Lopez, Phys. Rev. C, **52**, 3217 (1995)
11. M. Colona, Ph. Chomaz, A. Guarnera and B. Jacquot, Phys. Rev. C, **51**, 2671 (1995)
12. V.A. Karnaukhov et al., JINR, **E7-95-321**, Dubna, 1995; V.A. Karnaukhov et al., JINR, **E1-96-50**, Dubna, 1996
13. W. Bauer et al., Phys. Rev. C, **47**, 1838 (1993); S.C. Jeong et al., Phys. Rev. Lett., **72**, 3468 (1994); W.C. Hsi et al., Phys. Rev. Lett., **73**, 3367 (1994); M.A. Lisa et al., Phys. Rev. Lett., **75**, 2662 (1995); FOPI Collaboration., G. Poggi et al., Nucl. Phys. A, **586**, 755 (1995)
14. A.S. Botvina and D.H.E. Gross, Nucl. Phys. A, **592**, 257 (1995)
15. P.L. Jain, G. Singh, A. Mukhopadhyay, Phys. Rev. C, **50**, 1085 (1994)
16. M.L. Cherry et al. (The KLMM Collaboration), Phys. Rev. C, **52**, 2652 (1995)
17. C.B. Chitwood et al., Phys. Rev. C, **34**, 858 (1986); H.H. Gutbrod et al., Phys. Rev. C, **42**, 640 (1990); W.K. Wilson et al., Phys. Rev. C, **45**, 738 (1992); M.B. Tsang et al., Phys. Rev. C, **47**, 2717 (1993); L. Phair et al., Nucl. Phys. A, **564**, 453 (1993). A. Kugler et al., Phys. Lett. B, **335**, 319 (1994); R. Popescu et al., Phys. Rev. C, **54**, 796 (1996)
18. V.I. Zagrebaev and Yu.E. Penoinzhkevich, Phys. Part. Nucl. **24(2)**, 125 (1993)
19. Y. Yariv and Z. Fraenkel, Phys. Rev. C, **20**, 2227 (1979); ibig., **24**, 488 (1981); J.Cugnon, T. Mizutani, and J. Vandermeulen, Nucl. Phys. A, **352**, 505 (1981); J.Cugnon, D. Kinet, and J. Vandermeulen, Nucl. Phys. A, **379**, 553 (1982); ibig, **462**, 751 (1987); V.D. Toneev and K.K Gudima, Nucl. Phys. A, **400**, 173 (1983); Y. Pang, T.J. Schlagel, and S.H. Kahana, Nucl. Phys. A, **544**, 435 (1992)
20. M.I. Adamovich et al. (EMU-01 Collaboration), Zeit. fur Phys. A **358**, (1997) 357
21. H. Sorge, H. Stöcker, and W. Greiner, Ann. of Phys. (N.Y.), **192**, 266 (1989); H. Sorge, H. Stöcker, and W. Greiner, Nucl. Phys. A, **498**, 567c (1989); H. Sorge, A. v. Kretz, R. Mattiello, H. Stöcker, and W. Greiner, Zeit. Phys. C, **47**, 629 (1990); H. Sorge, L.A. Winckelmann, H. Stöcker, and W. Greiner, Zeit. Phys. C, **59**, 85 (1993)
22. T. Maruyama, T. Maruyama, K. Niita, Phys. Lett. B, **385** 34 (1995)
23. Kh. El-Waged and V.V. Uzhinskii, Yad. Fiz. **60** No. 5 (1997); JINR, **E2-94-126**, Dubna, 1994
24. Powell C.F., Fowler P.H., Perkins D.H. "The study of elementary particles by the photographic method", Pergamon Press, 1959
25. E. Fermi, Progr. Theor. Phys., **5**, 570 (1950)
26. V. Weisskopf, Phys. Rev., **56**, 426 (1936)
27. A.S. Botvina et al., Nucl. Phys. A, **475**, 663 (1987)
28. B. Andersson et al., Nucl. Phys. B, **281** 289 (1987); B. Nilsson-Almquist and E. Stenlund, Comp. Phys. Comm., **43**, 387 (1987)
29. K. Werner, Phys. Rep., **232**, 87 (1993)
30. X.-N. Wang and M. Gyulassy, Phys. Rev. C, **44**, 3501 (1991)
31. M.I. Adamovich et al. (EMU-01 Collaboration), Phys. Lett. B **363**,230 (1995)
32. T. Barnes, S. Capstick, M.D. Kovarik and E.S. Swanson, Phys. Rev. C, **48**, 539 (1993)
33. A. Bialas, M. Bleszynski, and W. Czyz, Nucl. Phys. B, **111**, 461 (1976)
34. S.Yu. Shmakov, V.V. Uzhinskii, and A.M. Zadorozhny, Comp. Phys. Comm., **54**, 125 (1989)
35. V. Flaminio, W.G. Moorhead, D.R.O. Morrison, and N. Rivoire, "Compilation of Cross-Sections III: p and $\hat{p}$ Induced Reactions", CERN-HERA 84-01 (1984)
36. G. Singh and P.L. Jain, Zeit. fur Phys. A, **348**, 99 (1994)
37. M.I. Adamovich et al. (EMU-01 Collaboration), Phys. Lett. B, **338**, 397 (1994)
38. M.L. Cherry et al. (The KLMM Collaboration), Report INP No. 1742/PH, Krakow, 1996
39. L.G. Dakhno and N.N. Nikolaev, Nucl. Phys. A, **436**, 653 (1985)
40. L.A. Kondratyuk and M.Zh. Shmatikov, Zeit. fur Phys. A, **321**, 301 (1985)
41. H. Feshbach and K. Huang, Phys. Lett. B, **47**, 300 (1973); A.S. Goldhaber, Phys. Lett. B, **53**, 306 (1974)
42. J.D. Bjorken and S.J. Brodsky, Phys. Rev. D, **1**, 1416 (1970)
43. A.S. Botvina, K.K. Gudima, A.S. Iljinov and I.N. Mishustin, Yad. Fiz., **57**, 667 (1994), (Physics of Atomic Nuclei, **57**, 689 (1994))
44. S. Yu. Shmakov et al., Yad. Fiz., **58**, 1735 (1995)